# Circuit Architecture of VTA Dopamine Neurons Revealed by Systematic Input–Output Mapping

**Kevin T. Beier**[1,2], **Elizabeth E. Steinberg**[2], **Katherine E. DeLoach**[1], **Stanley Xie**[1], **Kazunari Miyamichi**[1,5], **Lindsay Schwarz**[1], **Xiaojing J. Gao**[1,6], **Eric J. Kremer**[3,4], **Robert C. Malenka**[2,*], and **Liqun Luo**[1,*]

[1]Howard Hughes Medical Institute and Department of Biology, Stanford University, Stanford, CA 94305, USA

[2]Nancy Pritzker Laboratory, Department of Psychiatry and Behavioral Sciences, Stanford University School of Medicine, Stanford, CA 94305

[3]Institut de Génétique Moléculaire de Montpellier, CNRS 5535, 34293 Montpellier, France

[4]Université de Montpellier, 34000 Montpellier, France

## SUMMARY

Dopamine (DA) neurons in the midbrain ventral tegmental area (VTA) integrate complex inputs to encode multiple signals that influence motivated behaviors via diverse projections. Here we combine axon-initiated viral transduction with rabies-mediated transsynaptic tracing and Cre-based cell type-specific targeting to systematically map input–output relationships of VTA-DA neurons. We found that VTA-DA (and VTA-GABA) neurons receive excitatory, inhibitory, and modulatory input from diverse sources. VTA-DA neurons projecting to different forebrain regions exhibit specific biases in their input selection. VTA-DA neurons projecting to lateral and medial nucleus accumbens innervate largely non-overlapping striatal targets, with the latter also sending extra-striatal axon collaterals. Using electrophysiology and behavior, we validated new circuits identified in our tracing studies, including a previously unappreciated top-down reinforcing circuit from anterior cortex to lateral nucleus accumbens via VTA-DA neurons. This study highlights the utility of our viral-genetic tracing strategies to elucidate the complex neural substrates that underlie motivated behaviors.

## Graphical Abstract

---

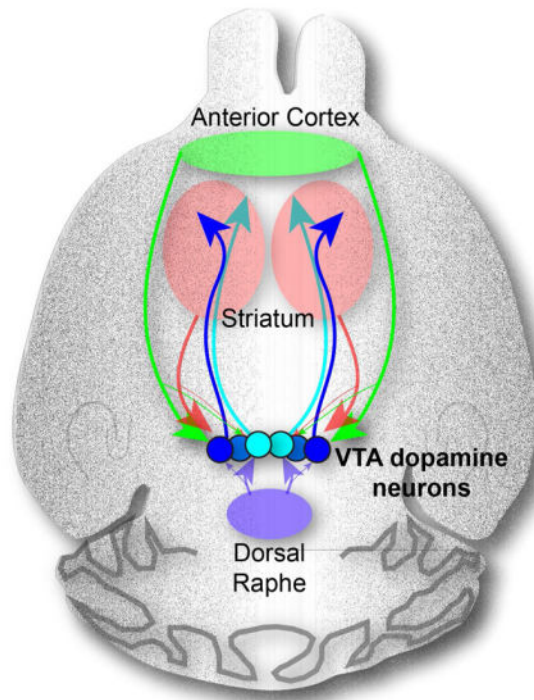*Corresponding authors (malenka@stanford.edu; lluo@stanford.edu).
[5]Department of Applied Biological Chemistry, Graduate School of Agricultural and Life Sciences, The University of Tokyo, Tokyo 113-8657, Japan
[6]Division of Biology, California Institute of Technology, Pasadena, CA 91125, USA

## INTRODUCTION

Dopamine (DA) neuron dysfunction has been implicated in numerous brain disorders, including addiction, depression, schizophrenia, and Parkinson's disease. Our incomplete understanding of the complex brain circuits in which dopamine neurons participate represents a major obstacle to developing more sophisticated hypotheses and improved treatments for these disorders. In the mammalian brain, the majority of DA neurons are clustered in two adjacent midbrain regions, the ventral tegmental area (VTA) and substantia nigra pars compacta (SNc). Initial in vivo electrophysiological studies suggested that midbrain DA neurons were a homogenous population, uniformly excited by rewards or reward-predictive cues, and unaffected or transiently inhibited by aversive events (Mirenowicz and Schultz 1996; Ungless et al., 2004). These findings were consistent with behavioral evidence demonstrating an unequivocal relationship between DA transmission and the reinforcing effects of natural and drug rewards (Wise and Rompré, 1989). However, the simplifying assumption that DA neurons functioned as a homogenous unit was called into question as data emerged that were inconsistent with this account. Although most DA neurons were activated by rewards and reward-predictive cues, some were activated by noxious or salient stimuli (Brischoux et al., 2009; Matsumoto and Hikosaka, 2009; Zweifel et al., 2011). Furthermore, important roles for DA neurons were uncovered in numerous behavioral or psychological processes other than reward, including salience, aversion, fear, working memory, and movement coordination (Bromberg-Martin et al., 2010; Jin and Costa, 2010; Zweifel et al., 2011; Lammel et al., 2012; Matsumoto and Takada, 2013). Heterogeneity was also detected at the cellular level, as subpopulations of DA neurons were

found to have distinct intrinsic molecular and electrophysiological properties (Margolis et al., 2006a, 2008; Lammel et al., 2008, 2011).

While a consensus is emerging that DA neurons are best conceptualized as functionally heterogeneous subpopulations capable of influencing diverse behavioral states (Bromberg-Martin et al., 2010; Roeper, 2013; Marinelli and McCutcheon, 2014), the underlying organizational principles that account for this heterogeneity remain unclear. Such principles would be especially useful in understanding the function of the VTA, which is cytochemically more diverse than the SNc (Margolis et al., 2006b). In addition to DA neurons, the VTA contains neurons that release GABA, glutamate, and their various combinations, all of which form local and long-range connections (Swanson, 1982; Fields et al., 2007; Morales and Root, 2014; Root et al., 2014). The anatomical location of a DA neuron's synaptic inputs and/or outputs may be a key determinant of its intrinsic properties and behavioral roles (Lammel et al., 2008; Margolis et al., 2008; Lammel et al., 2011, 2012). Thus, a comprehensive map detailing both the input and output connections of VTA-DA neurons would be of great value in deducing principles of midbrain circuit function.

Previous studies have sought to separately identify either the sources of synaptic inputs to VTA neurons (Phillipson, 1979; Carr and Sesack, 2000; Zahm et al., 2011; Watabe-Uchida et al., 2012), or the projection targets of these cells (Beckstead et al., 1979; Swanson, 1982). However, these experiments have two major limitations. First, synaptic inputs to the two main classes of VTA neurons (DA and GABA neurons) have not been comparatively evaluated at the whole-brain level. VTA-DA and VTA-GABA neurons have distinct firing patterns in vivo (Cohen et al., 2012), and their optogenetic activation produces opposing behavioral effects (Tsai et al., 2009; Tan et al., 2012). Thus, a systematic, comparative analysis of synaptic input onto VTA-DA and VTA-GABA neurons could be informative in elucidating general organizational principles that permit interdigitated neurons to make distinct contributions to brain function.

A second limitation has been an inability to systematically link information about a VTA-DA neuron's inputs with its projection targets. While such input–output relationships can be established in ultrastructural studies (e.g., Carr and Sesack, 2000), the methods involved are labor-intensive and thus cannot practically be scaled up to elucidate whole-brain input–output maps. Accordingly, only a handful of three-node circuits involving VTA neurons have been identified, undoubtedly representing a small fraction of such connections.

To address these limitations, we utilized rabies virus-based and cell type-specific monosynaptic tracing techniques (Wickersham et al., 2007; Callaway and Luo, 2015), as well as a viral-genetic strategy that permits whole-brain mapping of input–output relationships of genetically defined neuronal populations (Schwarz et al., 2015). These methods allowed for the generation of a comprehensive, high-resolution map of the input and output connectivity of VTA-DA neurons, thereby revealing previously unappreciated connections, including an anterior cortex→VTA-DA→nucleus accumbens (NAc) circuit. Using optogenetics, electrophysiology, and in vivo pharmacology, we verify the functional relevance of this circuit by demonstrating its role in positive reinforcement. Collectively, our data demonstrate that the input–output relationships of VTA-DA neuron subpopulations are

complex yet decipherable. They provide a critical roadmap for the development of more sophisticated and testable hypotheses about the neural circuit substrates that mediate the diverse behavioral functions of the VTA, in particular its DA neurons, in adaptive and pathological behaviors.

## RESULTS

### VTA-DA and VTA-GABA Neurons Receive Direct Input from Similar Brain Regions

Rabies-mediated transsynaptic tracing has previously been used to map direct inputs to DA neurons in two major midbrain nuclei, the SNc and VTA (Watabe-Uchida et al., 2012). To comprehensively map input and output through the VTA, we first extended these studies by comparing direct inputs to both VTA-DA and VTA-GABA neurons, and then examined the cell types in the input regions that synapse onto these two VTA populations.

To restrict our analysis specifically to VTA-DA and VTA-GABA neurons we used *DAT-Cre* mice, in which Cre mimics the expression pattern of the plasma membrane <u>do</u>p<u>a</u>mine <u>t</u>ransporter (Bäckman et al., 2006; Lammel et al., 2015), and *GAD2-Cre* mice, in which Cre mimics the expression of glutamic <u>a</u>cid <u>d</u>ecarboxylase-2 (Taniguchi et al., 2011), an enzyme that coverts glutamate to GABA (Figure S1). Two adeno-associated viruses (AAVs), expressing respectively a Cre-dependent <u>T</u>VA (the receptor for viruses containing the avian EnvA envelope glycoprotein) fused with m<u>C</u>herry (TC) and a Cre-dependent rabies glycoprotein (G), were injected into the VTA of these mice (Figure 1A) (Miyamichi et al., 2013). Two weeks later, we injected EnvA-pseudotyped, *G* deleted, and GFP-expressing rabies virus (RV*dG*). RV*dG* could only infect TC-expressing mammalian cells due to the EnvA pseudotype. Co-expression of *G* enabled TC-expressing neurons to complement RV*dG* and produce infectious rabies viruses that spread to their presynaptic partners. Almost all starter cells (defined by co-expression of TC and GFP) in the *DAT-Cre* mice expressed tyrosine hydroxylase (TH, a marker for DA neurons) (Figure 1B; quantified in Figure 1P inset) whereas few starter cells in the VTA of *GAD2-Cre* mice co-expressed TH (Figure 1C; quantified in Figure 1P inset). Control experiments demonstrated that the rabies-mediated transsynaptic tracing depended on Cre recombinase, TC, and G expression (Figure S2). Together, these results validated the cell-type specificity for input tracing.

We comparatively evaluated the sources of synaptic inputs to VTA-DA and VTA-GABA neurons by examining the distribution of GFP-positive neurons across different brain regions. Consistent with previous results (Watabe-Uchida et al., 2012), VTA-DA (Figure 1D–O) and VTA-GABA (data not shown) neurons received direct synaptic inputs from diverse neuronal types in a wide range of brain regions. We quantified input neurons in 22 brain regions (see Supplemental Experimental Procedures for details), and calculated the proportion of inputs from each region for both *DAT-Cre-* and *GAD2-Cre*-based tracing (Figure 1P; Table S1). VTA-GABA neurons received proportionally more inputs from the anterior cortex and central amygdala (CeA), while VTA-DA neurons received more inputs from the paraventricular hypothalamus (PVH) and lateral hypothalamus (LH), although none of these differences were significant when corrected for multiple comparisons. These results suggest that VTA-DA and VTA-GABA neurons receive largely similar input from different brain regions.

## VTA-DA and VTA-GABA Neurons Receive Input from Diverse Cell Types

To explore whether differences may exist at the cellular level within each input region, we combined in-situ hybridization (ISH) with rabies tracing (Takatoh et al., 2013; Weissbourd et al., 2014) on three selected input regions: the PVH, LH, and dorsal raphe (DR), each of which contains heterogeneous neuronal populations that are implicated in reward-related behaviors.

In the PVH (Figure 2A), we used probes for genes encoding the precursors for the neuropeptides oxytocin and arginine vasopressin (AVP), which have been implicated in several behavioral processes including reward, fear, and anxiety (Stoop, 2012). However, it is unknown whether neurons producing these peptides directly synapse onto VTA neurons. Co-labeling of RV$dG$-GFP with probes corresponding to oxytocin or AVP was observed when tracing inputs to both VTA-DA and VTA-GABA neurons (Figure 2B). For those GFP$^+$ PVH neurons that synapsed onto VTA-DA neurons, ~6% each were oxytocin$^+$ and AVP$^+$ (Figure 2C). These fractions increased to ~13% each for oxytocin$^+$ and AVP$^+$ neurons that synapse onto VTA-GABA neurons (Figure 2C).

In the LH (Figure 2D), we used probes corresponding to the neuropeptides neurotensin (NT) and hypocretin (orexin), which also have been linked to reward-related behaviors (Korotkova et al., 2003; Kempadoo et al., 2013). NT$^+$ and orexin$^+$ neurons were labeled by RV$dG$-GFP in both *DAT-Cre* and *GAD2-Cre* mice, indicating that they synapse directly onto VTA-DA and VTA-GABA neurons (Figure 2E). Interestingly, both NT$^+$ and orexin$^+$ neurons exhibited a two-fold preference for DA neurons (Figure 2F).

The DR contains heterogeneous neuronal populations that utilize different neurotransmitters including serotonin, GABA, and glutamate (Weissbourd et al., 2014) and has recently been shown to send a reward signal to the VTA, largely through neurons that co-express both vGluT3 (a marker for a subset of glutamatergic neurons) and Tph2 (a serotonin neuron marker) (Liu et al., 2014; McDevitt et al., 2014). To determine the neurochemical identity of DR cells that synapse onto VTA-DA and VTA-GABA neurons, we used ISH probes designed to detect either (1) all 3 vesicular glutamate transporters (vGluT1/2/3), markers of excitatory glutamatergic neurons, (2) both glutamic acid decarboxylases (GAD1/2), markers of inhibitory GABAergic neurons, or (3) Tph2. All three populations contributed a large fraction of DR input to both VTA-DA and VTA-GABA neurons, with similar relative preferences (Figure 2G–I).

Taken together, these results indicate that VTA neurons receive complex synaptic inputs from excitatory, inhibitory, and modulatory (serotonergic and peptidergic) neurons. These inputs synapse onto both VTA-DA and VTA-GABA neurons with some quantitative differences in their preferences.

## TRIO and cTRIO Analyses Reveal Distinct Inputs onto VTA Neurons Based on Their Output

Previous studies have demonstrated considerable heterogeneity in the properties of VTA-DA neurons that correlates with the location to which VTA-DA neurons project (Lammel et al., 2008; Margolis et al., 2008). To investigate whether DA neurons projecting to different targets receive inputs from different brain areas, we utilized recently developed TRIO (for

Tracing Relationships between Input and Output) and cTRIO (for cell-type-specific TRIO) techniques (Schwarz et al., 2015). TRIO relies on the axonal uptake of *CAV-Cre*, a canine adenovirus vector expressing Cre recombinase that efficiently transduces axon terminals (Soudais et al., 2001). RV*dG*-mediated input tracing based on *CAV-Cre* injected at a projection site can reveal inputs to projection-defined VTA subpopulations (Figure S3A). cTRIO further refines input tracing to VTA-DA neurons that project to a specific output site by utilizing *CAV-FLEx$^{loxP}$-Flp* that expressed a Cre-dependent Flp recombinase in conjunction with AAVs expressing Flp-dependent TC and G in *DAT-Cre* mice (Figure 3A). Four major targets of DA neurons were selected for CAV injections: two subdivisions of the ventral striatum—lateral or medial nucleus accumbens (NAcLat, NAcMed), medial prefrontal cortex (mPFC), and amygdala (Amy) (Figure 3B; Figure S3B–E).

The starter cell locations in TRIO and cTRIO experiments were consistent with a topographic organization of VTA-DA neurons based on their projection targets (Lammel et al., 2008). Along the medial–lateral axis, starter cells for NAcLat-projecting neurons were more laterally distributed within the VTA compared to starter cells for NAcMed-projecting neurons, for example (Figures 3C, S3F, S4). Quantification of VTA starter cells based on TH staining revealed that these four groups contained different fractions of DA neurons in the TRIO experiments, ranging from ~90% for NAcLat-projecting to <50% for mPFC- and Amy-projecting VTA neurons (Figure S3C), consistent with previous studies using conventional tracers (Swanson, 1982). By contrast, >90% of the starter cells for all four groups were TH+ in cTRIO experiment (Figure 3D), validating the neurochemical specificity of the cTRIO strategy.

Both TRIO and cTRIO analyses revealed quantitative differences in the inputs onto VTA neurons according to their outputs (Figure S3H, Figure 3E); the variation in cTRIO experiments was smaller than for TRIO (Table S2) likely because starter cells were defined not only by projection but also cell type. We focus our discussion on cTRIO experiments because of the clear DA neuron identity. Notably, NAcLat-projecting VTA-DA neurons received proportionally more input from the anterior cortex, dorsal striatum, and nucleus accumbens core (NAcCore) and lateral shell (NAcLatS), but less input from the DR, than the three other VTA-DA populations. In contrast, NAcMed-projecting DA neurons received preferential input from the NAc medial shell (NAcMedS) at the expense of dorsal striatum (Figure 3E). These experiments demonstrate that VTA-DA neurons that project to different output sites receive biased input from selective regions, notably dorsal raphe and different striatal regions.

## NAcMed- and NAcLat-projecting DA Neurons Have Distinct Arborization Patterns

A striking finding from the TRIO and cTRIO analyses is that VTA-DA neurons that project to subdivisions of the ventral striatum (NAcMed vs. NAcLat) receive highly biased inputs from different brain regions. This suggests that these projections originate from largely different populations of DA neurons. Indeed, individual VTA-DA neurons have been suggested to innervate one selective projection target based on lack of co-labeling of retrograde tracers injected into different VTA projection sites (Fallon, 1981; Swanson, 1982; Margolis et al., 2006a; Lammel et al., 2008). However, this methodology may not detect all

axonal collateralizations because potential target regions can only be sampled 1–3 at a time. Additionally, incomplete coverage of the retrograde tracer within each sampled region may reduce the probability of detecting axon collateralization. To overcome these limitations, we employed an intersectional strategy to label VTA-DA neurons that project to a specific output target (Figure 4A) that allowed us to visualize directly axonal arbors of anatomically-defined DA neurons, permitting a more comprehensive analysis of the axonal collateralization (or lack thereof) of specific DA neuron subpopulations.

We injected *CAV-FLEx^loxP-Flp* into the NAcLat or NAcMed of *DAT-Cre* mice and an AAV expressing Flp-dependent membrane-tethered GFP (mGFP) into the VTA. This allowed examination of the axonal arborization pattern of NAcLat- or NAcMed-projecting VTA-DA neurons. Quantification of these axonal projections in 10 brain regions that contained projections from at least one of the four DA neuron subtypes examined revealed that the axon arbors of the NAcLat-projecting DA neurons largely avoided the NAc medial shell, while projecting more laterally and broadly in the striatum including the dorsal striatum (Figure 4B–C; quantified in Figure 4D). By contrast, axonal arbors of NAcMed-projecting VTA-DA neurons were highly enriched in the NAc medial shell (Figure 4B, quantified in Figure 4D) but largely avoided the NAc lateral shell. In total, NAcLat-projecting DA neurons had three-fold broader arborizations in the striatum than NAcMed-projecting DA neurons (Figure 4E). Very few axonal arbors were observed in the mPFC or central amygdala from either condition. Interestingly, while the axonal arbors of NAcLat-projecting DA neurons were largely confined to the striatum, NAcMed-projecting DA neurons sent significant collaterals outside the striatum, including the septum and ventral pallidum, indicating that this DA subpopulation is capable of simultaneously influencing neural activity in multiple brain regions.

### Electrophysiological Examination of Synaptic Connections Predicted by cTRIO

cTRIO analysis of the input–output relationships of VTA-DA neurons revealed several previously unrecognized connectivity patterns. To examine whether they represent functional connections, we performed ex vivo electrophysiological assays, in which we optically activated inputs expressing channelrhodopsin-2 (ChR2) while recording from identified DA neurons projecting to specific targets labeled with retrobeads (Lammel et al., 2012).

Previous work suggested that lateral habenula (LHb) neurons do not make synaptic connections onto VTA-DA neurons projecting to the NAcLat (Lammel et al., 2012) whereas cTRIO analysis suggests that LHb inputs comprised ~3% of all inputs to this population. To investigate this discrepancy, we injected an AAV expressing ChR2 into the LHb and red retrobeads into the NAcLat of transgenic mice in which DA neurons were GFP+ (Figure 5A). Whole-cell recordings were made from acute slices containing VTA neurons that were both green (DA+) and red (NAcLat-projecting). Photostimulation-evoked synaptic responses were observed in 2 of 26 recorded neurons (Figure 5B–D), which were blocked by the AMPA receptor antagonist CNQX. These observations are consistent both with previous observations that the LHb input to NAcLat-projecting VTA-DA neurons is sparse (0 of 4 cells; Lammel et al., 2012) and with our cTRIO results showing that such a connection

exists. The location of responding neurons may explain why previous electrophysiology studies may have missed this connection, as the responding cells were located more ventrally (Figure 5B) than expected for NAcLat-projecting DA neurons (Lammel et al., 2008). This example also illustrates that rabies-based transsynaptic techniques have the sensitivity to uncover relatively rare connections that could be missed using other techniques.

Another surprising cTRIO result is that the anterior cortex, including the mPFC, makes monosynaptic connections onto NAc-projecting DA neurons (Figure 3E). Previous electron microscopy studies using classical tracers suggested that mPFC inputs to the VTA synapse onto mPFC-projecting but not onto NAc-projecting DA neurons (Carr and Sesack, 2000). To investigate this discrepancy, we performed similar electrophysiological recordings to those just described but injected the AAV expressing ChR2 into the mPFC. 5 of 37 NAc-projecting VTA-DA neurons showed a time-locked response to photostimulation (Figure 5B–D), functionally validating a pathway identified by cTRIO. As our input tracing data demonstrated that anterior cortical input to VTA-DA neurons also arose from other frontal cortical regions besides the mPFC (Figure S5), in separate experiments we injected the AAV expressing ChR2 into broader anterior cortical regions, including the insular and orbitofrontal cortices in addition to the mPFC. In these mice, 19 of 36 NAc-projecting VTA-DA neurons showed a time-locked response to photostimulation that was blocked by CNQX. These connections also displayed a higher mean EPSC amplitude (28.4±7.7 pA for anterior cortex versus 14.9±3.0 pA for mPFC, Figure 5E), likely due to more anterior cortical cells expressing ChR2. Thus, signals arising from the anterior cortex are capable of influencing neural activity in a large proportion of NAcLat-projecting VTA-DA neurons.

## The Anterior Cortex→VTA-DA→NAcLat Circuit Is Reinforcing

We next asked what role the anterior cortex→VTA-DA→NAcLat circuit could play in behavior. As anterior cortex provided excitatory input onto NAcLat-projecting VTA-DA neurons in our slice recordings, we hypothesized that activation of anterior cortical inputs to the VTA in vivo would lead to DA release in the NAcLat, which would be reinforcing. To test this hypothesis, we injected mice with an AAV expressing either ChR2-eYFP (n=7) or eYFP alone (n=8) into the anterior cortex (including the mPFC, insular, and orbitofrontal cortices), and implanted optical fibers targeted just dorsal to the VTA (Figure 6A–B; Figure S6). After waiting 2–3 months, mice were subjected to an intracranial self-stimulation (ICSS) procedure during which they were allowed to respond freely at 5 adjacent nosepoke ports for photostimulation. Responses at 4 ports resulted in photostimulation of anterior cortex→VTA projections at varying stimulation frequencies (1, 5, 10, or 20 Hz) for 2s; responses at a 5th control port did not result in any stimulation (Figure 6C). ChR2-eYFP-expressing mice developed a strong preference for the 20-Hz port over successive training days, making significantly more responses at this port than at the control port that did not produce stimulation (Figure 6D). In contrast, eYFP-expressing control mice did not show this preference (Figure 6E–F).

To determine whether the reinforcing effects of the anterior cortex→VTA projection stimulation required DA release in the NAcLat, we combined site-specific pharmacology

with optogenetic manipulation. In a subset of high-responding ChR2-eYFP-expressing mice (n=5), we infused varying doses of flupenthixol, a non-selective DA receptor antagonist, or saline vehicle, into the NAcLat via previously implanted cannulas targeting this area (see Supplemental Experimental Procedures; Figures 6A; Figure S6). Flupenthixol infusion into the NAcLat prior to ICSS behavioral sessions resulted in a dose-dependent decrease in responding for 20-Hz stimulation of anterior cortex→VTA projections (Figure 6G), consistent with our hypothesis that optically-evoked DA release in NAcLat was a critical mediator of the ICSS behavior we observed. Flupenthixol infusion also reduced locomotion during ICSS sessions (Figure 6H). However, the latency to initiate response at the 20-Hz nosepoke port was unaffected (Figure 6I), indicating that mice were physically capable of making nosepoke responses under the influence of flupenthixol. Importantly, because behavioral sessions did not begin until >10 min after drug infusions were complete, DA receptors in the NAcLat were likely to be fully blocked at the beginning of the session when latency measurements were recorded.

Taken together, these data suggest that the anterior cortex makes direct, excitatory synaptic connections onto VTA-DA neurons projecting to the NAcLat, and that activation of this circuit is reinforcing.

## DISCUSSION

We have utilized rabies-mediated transsynaptic tracing and TRIO/cTRIO to dissect the complex circuits in which midbrain VTA-DA neurons participate. Our unbiased anatomical mapping revealed the global input–output architecture of the majority of VTA-DA neurons. We validated two previously unknown circuits with electrophysiology and identified a behavioral function of one of the new circuits. Below we discuss the technical and conceptual implications of these findings.

### Technical Considerations

Recent transsynaptic tracing techniques have permitted systematic, high-resolution analyses of inputs based on the location, genetic identity (cell type), or axonal projection of starter cells (Callaway and Luo, 2015). cTRIO simultaneously leverages all of these targeting strategies, thereby allowing access to more specific starter cell populations for dissecting complex circuits, such as those involving VTA-DA neurons. A previous method of labeling inputs based on outputs of VTA-DA neurons relied on RV*dG* injection directly into an output site, and trans-complementing the virus in VTA-DA neurons by expressing G under the control of *TH-Cre* (Lammel et al., 2012). A caveat of this method is that if RV*dG* spread among DA neurons, input–output specificity would be compromised, as all *TH-Cre*-expressing neurons would be competent to initiate transsynaptic tracing. As TRIO and cTRIO limit TC and G expression only to neurons projecting directly to the target site, the input–output relationship is preserved even if VTA-DA neurons are locally connected. In addition, TRIO and cTRIO produced about ten-fold more efficient labeling than the previous method (Lammel et al., 2012), thus identifying more comprehensive monosynaptic inputs to projection-based VTA-DA subpopulations.

The electrophysiological validations of new connections identified in our cTRIO experiments highlight the sensitivity of rabies-mediated transsynaptic tracing techniques. While previous electrophysiological (Lammel et al., 2012) and EM studies (Carr and Sesack, 2000) did not identify the LHb→VTA-DA→NAcLat or the mPFC→VTA-DA→NAcLat circuit, their presence in our cTRIO experiments motivated a further examination. Our observations support the hypothesis that the LHb sends a weak input to the NAcLat-projecting VTA-DA neurons. We also identified and validated direct synaptic connections from the mPFC onto VTA-DA neurons projecting to the NAc.

While EM and slice electrophysiology are powerful methods for studying circuit architecture and function, they are less suited for large-scale connectivity analyses. TRIO/ cTRIO provide a global "scaffold" to identify input–output architecture of a region and/or cell types of interest. The properties and function of the circuits can be further investigated using electrophysiology and optogenetics, as exemplified in our study. These combined approaches can be applied to many other cell types and circuits in the mammalian brain.

## Architecture of VTA-DA Circuitry

Our whole-brain transsynaptic tracing from VTA-DA and VTA-GABA neurons have extended previous findings (Watabe-Uchida et al., 2012). We observed that both types of neurons receive inputs from a wide variety of brain regions, with overall similar distributions (Figure 1). This is reminiscent of our recent input-tracing study in the dorsal raphe (DR), where serotonin and GABA neurons receive qualitatively similar input from diverse brain regions (Weissbourd et al., 2014). This common feature could be used for input to VTA or DR GABA neurons to serve as feed-forward inhibition to regulate the activity of DA or serotonin neurons. As is the case for DR-serotonin and -GABA neurons, VTA-DA and -GABA neurons receive diverse direct input from excitatory, inhibitory, and modulatory neurons, including prominent direct input from DR serotonin and GABA neurons (Figure 2), highlighting the complex regulation of these neuromodulatory systems and their rich interactions.

In addition to the complex input patterns, VTA-DA neurons project to diverse output sites that appear to correlate with their intrinsic properties, cell body location, and, in one specific example, input preference (Lammel et al., 2008, 2011, 2012). Our TRIO/cTRIO analyses have provided a comprehensive overview of the input–output relationships of multiple subtypes of VTA-DA neurons projecting to four principal output sites: the nucleus accumbens (NAcMed, NAcLat), medial prefrontal cortex, and amygdala. Our data confirmed a correlation between VTA output sites and the location of the cell soma within the VTA (Figure S4). At the same time, these data have produced a more nuanced picture of the input–output relationships of this complex structure than the discrete pathways suggested by a previous study (Lammel et al., 2012), likely reflecting the sensitivity of the TRIO techniques (see above). Qualitatively, VTA-DA neurons projecting to all output sites receive input from all 22 brain regions examined in this study. Quantitatively, however, input patterns can be highly biased depending on the output sites (Figures 3 & S3). NAcLat-projecting VTA-DA neurons have the most distinct input patterns compared with all three other groups of VTA-DA neurons. Furthermore, our axonal arborization analysis (Figure 4)

demonstrates that NAcLat-projecting VTA-DA neurons have little overlap with NAcMed-projecting VTA-DA neurons in their striatal target regions, and that NAcMed-projecting VTA-DA neurons have previously unknown extra-striatal collateralization. Thus, our data support a biased-input/discrete output architecture for VTA-DA circuitry. A similar input–output architecture also applies to SNc-DA circuitry (Lerner et al., 2015; companion paper).

As the major output site of VTA-DA neurons and a crucial structure implicated in reward processing and drug addiction, the nucleus accumbens has been intensively studied. However, NAc-projecting DA neurons have been considered a homogeneous population. Our data demonstrate that NAcMed- and NAcLat-projecting VTA-DA neurons represent two discrete populations with distinct targets and receive differential inputs. NAcLat-projecting VTA-DA neurons preferentially receive input from the anterior cortex and striatal regions, whereas NAcMed-projecting VTA-DA neurons preferentially receive input from the dorsal raphe (Figure 3E). Together with the differential gene expression and firing patterns, these observations strongly suggest that these DA neuron subpopulations are integrated into different circuits and serve distinct biological functions. These findings highlight the importance of differentiating DA neuron subpopulations and NAc sub-regions where possible in future studies.

The observations of discrete outputs and specific input–output relationships for VTA-DA neurons contrast with the architecture of locus coeruleus norepinephrine (LC-NE) circuits. LC-NE neurons received similar inputs regardless of where they project, and projection-defined subpopulations of LC-NE neurons also project to all brain regions examined (Schwarz et al., 2015). While these catecholamine circuits have sometimes been treated as complementary systems, with the DA neurons projecting to the striatum and NE neurons elsewhere, their input–output structures are markedly different. The NE circuit architecture is consistent with a role to "broadcast" a general message throughout the brain, which may be optimal for coordinating brain states such as sleep and arousal. The DA system is better suited for sending discrete signals. For example, subpopulations of VTA-DA neurons have previously been found to differentially encode reward and aversion in mice (Lammel et al., 2012) and non-human primates (Matsumoto and Hikosaka, 2009). Indeed, the circuit architecture of using parallel channels to encode discrete information may be evolutionarily conserved; recent studies have identified unique populations of *Drosophila* DA neurons carrying appetitive or aversive signals that project to discrete zones of the mushroom body, an insect center for learning and memory (Aso et al., 2014).

### A Top-Down Reinforcement Signal

In this study, we identified a behavioral function of a previously unappreciated connection from the anterior cortex to NAcLat-projecting VTA-DA neurons. While prior work demonstrated that altering activity in the PFC changes DA levels in the striatum (e.g., Karreman and Moghaddam, 1996), other data suggested that a direct mPFC→VTA-DA→NAcLat circuit did not exist (Carr and Sesack, 2000). Our cTRIO studies revealed a monosynaptic connection from the anterior cortex to NAcLat-projecting DA neurons, a finding that we confirmed with ex vivo electrophysiological recordings from identified NAcLat-projecting VTA-DA neurons. Using optogenetics and behavioral pharmacology, we

identified a functional role for this circuit in mediating positive reinforcement. Thus, our data suggest that frontal cortical regions are capable of exerting top-down control of midbrain neurons that contribute to motivated behaviors via DA release in the NAc, bypassing other intermediary regions such as the LDT and striatum to directly engage DA neurons and exert executive control over a powerful neuromodulatory system.

In summary, our data add to a growing body of evidence in favor of a model wherein functionally distinct midbrain DA neuron subtypes encode different signals and participate in largely separate yet interconnected circuits through their biased input and discrete output pathways. However, much remains to be understood. For example, investigating the circuit properties of NAc inputs onto both DA and GABA neurons (feedback and feed-forward inhibition), and defining the message encoded in the firing patterns of each of these DA neuron subpopulations in response to various natural stimuli, will be necessary to understand the normal and pathophysiological functions of these important circuits.

## EXPERIMENTAL PROCEDURES

### Mice and Viral Procedures

*DAT-Cre* (Bäckman et al., 2006), tdTomato Cre reporter *Ai14* (Madisen et al., 2010), and C57Bl/6 mice were obtained from the Jackson Laboratories, and *GAD2-Cre* mice (Taniguchi et al., 2011) were from Josh Huang. Mice were housed on a 12-hour light/dark cycle with food and water *ad libitum*. Viral vectors were prepared as previously described (Schwarz et al., 2015). Detailed procedures for rabies tracing, TRIO, cTRIO and axonal arborization are described in Supplemental Experimental Procedures. All procedures followed animal care and biosafety guidelines approved by Stanford University's Administrative Panel on Laboratory Animal Care and Administrative Panel of Biosafety.

### Electrophysiology

Six-week old *DAT-Cre* mice were injected with $AAV_1$-*CMV-FLEx-GFP* into the VTA, rhodamine-conjugated retrobeads into NAcLat, and $AAV_{DJ}$-*hsyn1-ChR2-H134R-eYFP* into the LHb, mPFC, or anterior cortex. 8 weeks later, recordings were done as previously described (Lammel et al., 2011). Excitatory postsynaptic currents (EPSCs) were recorded in whole-cell voltage clamp; series resistance and input resistance were monitored on-line with a 4-mV hyperpolarizing step (50 ms). Neurons were voltage-clamped at –60 mV to record AMPAR EPSCs. For drug application, CNQX (10 µM) was added to the ACSF. Connections were defined as neurons that exhibited an average current (over 5 sweeps) of 10 pA recorded either at –60 mV or +40 mV.

### Behavior

$AAV_5$-*hsyn1-eYFP* or $AAV_5$-*hsyn1-ChR2-eYFP* (0.5 µL) was infused bilaterally into the anterior cortex of C57Bl/6 mice. Optical fibers were implanted dorsal to the VTA, and cannulas were implanted targeting the NAcLat. >8 weeks following virus infusions, ChR2-eYFP mice and eYFP controls were given 5 daily ICSS training sessions during which they could respond at 5 nosepoke ports. A response at each port produced 2s of 473nm light, pulsed at a particular frequency (20, 10, 5, 1, or 0 Hz). Following ICSS training, a subset of

high-responding ChR2-eYFP mice was used for drug infusion studies. These mice received bilateral 0.25 μL infusions of either flupenthixol (F114, Sigma, dissolved in saline) or saline vehicle through the implanted guide cannula 10 minutes prior to ICSS sessions.

## Statistical Analysis

Results of all statistical analyses for tracing experiments are provided in Table S2. For each input brain region, paired t-tests were used for input tracing and ISH experiments, and one-way ANOVAs were used for TRIO and cTRIO data, with correction for multiple comparisons. (We did not use 2-way ANOVA because the data from different brain regions did not meet equal variance assumption.) For starter cell distributions, t-tests were used with corrections for multiple comparisons. Behavioral data were analyzed with parametric or non-parametric one-way repeated-measures ANOVAs followed by Holm-Sidak or Tukey post-hoc tests.

## Supplementary Material

Refer to Web version on PubMed Central for supplementary material.

## Acknowledgments

## References

Aso Y, Hattori D, Yu Y, Johnston RM, Iyer Nirmala A, Ngo T-T, Dionne H, Abbott LF, Axel R, Tanimoto H, et al. The neuronal architecture of the mushroom body provides a logic for associative learning. Elife. 2014:1–47.

Bäckman CM, Malik N, Zhang Y, Shan L, Grinberg A, Hoffer BJ, Westphal H, Tomac AC. Characterization of a mouse strain expressing Cre recombinase from the 3′ untranslated region of the dopamine transporter locus. Genesis. 2006; 44:383–390. [PubMed: 16865686]

Beckstead RM, Domesick VB, Nauta WJ. Efferent connections of the substantia nigra and ventral tegmental area in the rat. Brain Res. 1979; 175:191–217. [PubMed: 314832]

Brischoux F, Chakraborty S, Brierley DI, Ungless MA. Phasic excitation of dopamine neurons in ventral VTA by noxious stimuli. Proc Natl Acad Sci U S A. 2009; 106:4894–4899. [PubMed: 19261850]

Bromberg-Martin ES, Matsumoto M, Hikosaka O. Dopamine in motivational control: rewarding, aversive, and alerting. Neuron. 2010; 68:815–834. [PubMed: 21144997]

Callaway EM, Luo L. Monosynaptic circuit tracing with glycoprotein-deleted rabies viruses. J Neurosci. 2015; 35:8979–8985. [PubMed: 26085623]

Carr DB, Sesack SR. Projections from the rat prefrontal cortex to the ventral tegmental area: target specificity in the synaptic associations with mesoaccumbens and mesocortical neurons. J Neurosci. 2000; 20:3864–3873. [PubMed: 10804226]

Cohen JY, Haesler S, Vong L, Lowell BB, Uchida N. Neuron-type specific signals for reward and punishment in the ventral tegmental area. Nature. 2012; 482:85–88. [PubMed: 22258508]

Fallon J. Collateralization of monoammine neurons: mesotelencephalic dopamine projections to caudate, septum, and frontal cortex. J Neurosci. 1981; 1:1361–1368. [PubMed: 6172572]

Fields HL, Hjelmstad GO, Margolis EB, Nicola SM. Ventral tegmental area neurons in learned appetitive behavior and positive reinforcement. Annu Rev Neurosci. 2007; 30:289–316. [PubMed: 17376009]

Jin X, Costa RM. Start/stop signals emerge in nigrostriatal circuits during sequence learning. Nature. 2010; 466:457–462. [PubMed: 20651684]

Karreman M, Moghaddam B. The prefrontal cortex regulates the basal release of dopamine in the limbic striatum: an effect mediated by ventral tegmental area. J Neurochem. 1996; 66:589–598. [PubMed: 8592128]

Kempadoo KA, Tourino C, Cho SL, Magnani F, Leinninger GM, Stuber GD, Zhang F, Myers MG, Deisseroth K, de Lecea L, et al. Hypothalamic neurotensin projections promote reward by enhancing glutamate transmission in the VTA. J Neurosci. 2013; 33:7618–7626. [PubMed: 23637156]

Korotkova TM, Sergeeva OA, Eriksson KS, Haas HL, Brown RE. Excitation of ventral tegmental area dopaminergic and nondopaminergic neurons by orexins/hypocretins. J Neurosci. 2003; 23:7–11. [PubMed: 12514194]

Lammel S, Hetzel A, Hackel O, Jones I, Liss B, Roeper J. Unique properties of mesoprefrontal neurons within a dual mesocorticolimbic dopamine system. Neuron. 2008; 57:760–773. [PubMed: 18341995]

Lammel S, Ion DI, Roeper J, Malenka RC. Projection-specific modulation of dopamine neuron synapses by aversive and rewarding stimuli. Neuron. 2011; 70:855–862. [PubMed: 21658580]

Lammel S, Lim BK, Ran C, Huang KW, Betley MJ, Tye KM, Deisseroth K, Malenka RC. Input-specific control of reward and aversion in the ventral tegmental area. Nature. 2012; 491:212–217. [PubMed: 23064228]

Lammel S, Steinberg EE, Foldy C, Wall NR, Beier K, Luo L, Malenka RC. Diversity of Transgenic Mouse Models for Selective Targeting of Midbrain Dopamine Neurons Matters Arising Diversity of Transgenic Mouse Models for Selective Targeting of Midbrain Dopamine Neurons. Neuron. 2015; 85:429–438. [PubMed: 25611513]

Lerner, TN.; Shilyansky, C.; Davidson, TJ.; Evans, KE.; Beier, KT.; Zalocusky, KA.; Crow, AK.; Malenka, RC.; Luo, L.; Tomer, R., et al. Intact-brain analyses reveal distinct information carried by SNc dopamine subcircuits. 2015. Submitted (companion manuscript)

Liu Z, Zhou J, Li Y, Hu F, Lu Y, Ma M, Feng Q, Zhang JE, Wang D, Zeng J, et al. Dorsal raphe neurons signal reward through 5-HT and glutamate. Neuron. 2014; 81:1360–1374. [PubMed: 24656254]

Madisen L, Zwingman TA, Sunkin SM, Oh SW, Zariwala HA, Gu H, Ng LL, Palmiter RD, Hawrylycz MJ, Jones AR, et al. A robust and high-throughput Cre reporting and characterization system for the whole mouse brain. Nat Neurosci. 2010; 13:133–140. [PubMed: 20023653]

Margolis EB, Lock H, Chefer VI, Shippenberg TS, Hjelmstad GO, Fields HL. κ opioids selectively control dopaminergic neurons projecting to the prefrontal cortex. Proc Natl Acad Sci U S A. 2006a; 103:2938–2942. [PubMed: 16477003]

Margolis EB, Lock H, Hjelmstad GO, Fields HL. The ventral tegmental area revisited: is there an electrophysiological marker for dopaminergic neurons? J Physiol. 2006b; 577:907–924. [PubMed: 16959856]

Margolis EB, Mitchell JM, Ishikawa J, Hjelmstad GO, Fields HL. Midbrain dopamine neurons: projection target determines action potential duration and dopamine D(2) receptor inhibition. J Neurosci. 2008; 28:8908–8913. [PubMed: 18768684]

Marinelli M, McCutcheon JE. Heterogeneity of dopamine neuron activity across traits and states. Neuroscience. 2014; 282:176–197. [PubMed: 25084048]

Matsumoto M, Hikosaka O. Two types of dopamine neuron distinctly convey positive and negative motivational signals. Nature. 2009; 459:837–841. [PubMed: 19448610]

Matsumoto M, Takada M. Distinct representations of cognitive and motivational signals in midbrain dopamine neurons. Neuron. 2013; 79:1011–1024. [PubMed: 23932490]

McDevitt RA, Tiran-Cappello A, Shen H, Balderas I, Britt JP, Marino RAM, Chung SL, Richie CT, Harvey BK, Bonci A. Serotonergic versus nonserotonergic dorsal raphe projection neurons: differential participation in reward circuitry. Cell Rep. 2014; 8:1857–1869. [PubMed: 25242321]

Mirenowicz J, Schultz W. Preferential activation of midbrain dopamine neurons by appetitive rather than aversive stimuli. Nature. 1996; 379:449–451. [PubMed: 8559249]

Miyamichi K, Shlomai-Fuchs Y, Shu MM, Weissbourd BC, Luo L, Mizrahi A. Dissecting local circuits: parvalbumin interneurons underlie broad feedback control of olfactory bulb output. Neuron. 2013; 80:1232–1245. [PubMed: 24239125]

Morales M, Root DH. Glutamate neurons within the midbrain dopamine regions. Neuroscience. 2014; 282:60–68. [PubMed: 24875175]

Phillipson OT. Afferent projections to the ventral tegmental area of Tsai and interfascicular nucleus: a horseradish peroxidase study in the rat. J Comp Neurol. 1979; 187:117–143. [PubMed: 489776]

Roeper J. Dissecting the diversity of midbrain dopamine neurons. Trends Neurosci. 2013; 36:336–342. [PubMed: 23582338]

Root DH, Mejias-Aponte CA, Zhang S, Wang H-L, Hoffman AF, Lupica CR, Morales M. Single rodent mesohabenular axons release glutamate and GABA. Nat Neurosci. 2014; 17:1543–1551. [PubMed: 25242304]

Schwarz LA, Miyamichi K, Gao XJ, Beier KT, Weissbourd B, DeLoach KE, Ren J, Ibanes S, Malenka RC, Kremer EJ, et al. Viral-genetic tracing of the input–output organization of a central noradrenaline circuit. Nature. 201510.1038/nature14600

Soudais C, Laplace-Builhe C, Kissa K, Kremer EJ. Preferential transduction of neurons by canine adenovirus vectors and their efficient retrograde transport in vivo. FASEB J. 2001; 15:2283–2285. [PubMed: 11511531]

Stoop R. Neuromodulation by oxytocin and vasopressin. Neuron. 2012; 76:142–159. [PubMed: 23040812]

Swanson LW. The projections of the ventral tegmental area and adjacent regions: a combined fluorescent retrograde tracer and immunofluorescence study in the rat. Brain Res Bull. 1982; 9:321–353. [PubMed: 6816390]

Takatoh J, Nelson A, Zhou X, Bolton MM, Ehlers MD, Arenkiel BR, Mooney R, Wang F. New modules are added to vibrissal premotor circuitry with the emergence of exploratory whisking. Neuron. 2013; 77:346–360. [PubMed: 23352170]

Tan KR, Yvon C, Turiault M, Mirzabekov JJ, Doehner J, Labouèbe G, Deisseroth K, Tye KM, Lüscher C. GABA neurons of the VTA drive conditioned place aversion. Neuron. 2012; 73:1173–1183. [PubMed: 22445344]

Taniguchi H, He MH, Wu P, Kim S, Paik R, Sugino K, Kvitsani D, Fu Y, Lu JL, Lin Y, et al. A resource of Cre driver lines for genetic targeting of GABAergic neurons in cerebral cortex. Neuron. 2011; 71:995–1013. [PubMed: 21943598]

Tsai HC, Zhang F, Adamantidis A, Stuber GD, Bonci A, de Lecea L, Deisseroth K. Phasic firing in dopaminergic neurons is sufficient for behavioral conditioning. Science. 2009; 324:1080–1084. [PubMed: 19389999]

Ungless MA, Magill PJ, Bolam JP. Uniform inhibition of dopamine neurons in the ventral tegmental area by aversive stimuli. Science. 2004; 303:2040–2042. [PubMed: 15044807]

Watabe-Uchida M, Zhu L, Ogawa SK, Vamanrao A, Uchida N. Whole-brain mapping of direct inputs to midbrain dopamine neurons. Neuron. 2012; 74:858–873. [PubMed: 22681690]

Weissbourd B, Ren J, DeLoach KE, Guenthner CJ, Miyamichi K, Luo L. Presynaptic partners of dorsal raphe serotonergic and GABAergic neurons. Neuron. 2014; 83:645–662. [PubMed: 25102560]

Wickersham IR, Lyon DC, Barnard RJO, Mori T, Finke S, Conzelmann KK, Young JAT, Callaway EM. Monosynaptic restriction of transsynaptic tracing from single, genetically targeted neurons. Neuron. 2007; 53:639–647. [PubMed: 17329205]

Wise RA, Rompré P-P. Brain dopamine and reward. Annu Rev Psychol. 1989; 40:191–225. [PubMed: 2648975]

Zahm DS, Cheng AY, Lee TJ, Ghobadi CW, Schwartz ZM, Geisler S, Parsely KP, Gruber C, Veh RW. Inputs to the midbrain dopaminergic complex in the rat, with emphasis on extended amygdala-recipient sectors. J Comp Neurol. 2011; 519:3159–3188. [PubMed: 21618227]

Zweifel LS, Fadok JP, Argilli E, Garelick MG, Jones GL, Dickerson TMK, Allen JM, Mizumori SJY, Bonci A, Palmiter RD. Activation of dopamine neurons is critical for aversive conditioning and prevention of generalized anxiety. Nat Neurosci. 2011; 14:620–626. [PubMed: 21499253]

## Article Highlights

VTA dopamine (DA) and GABA neurons receive similar inputs from diverse sources

VTA-DA neurons projecting to different output sites receive biased input

VTA-DA neurons projecting to lateral and medial NAc innervate non-overlapping targets

A top-down anterior cortex→VTA-DA→lateral NAc circuit is reinforcing
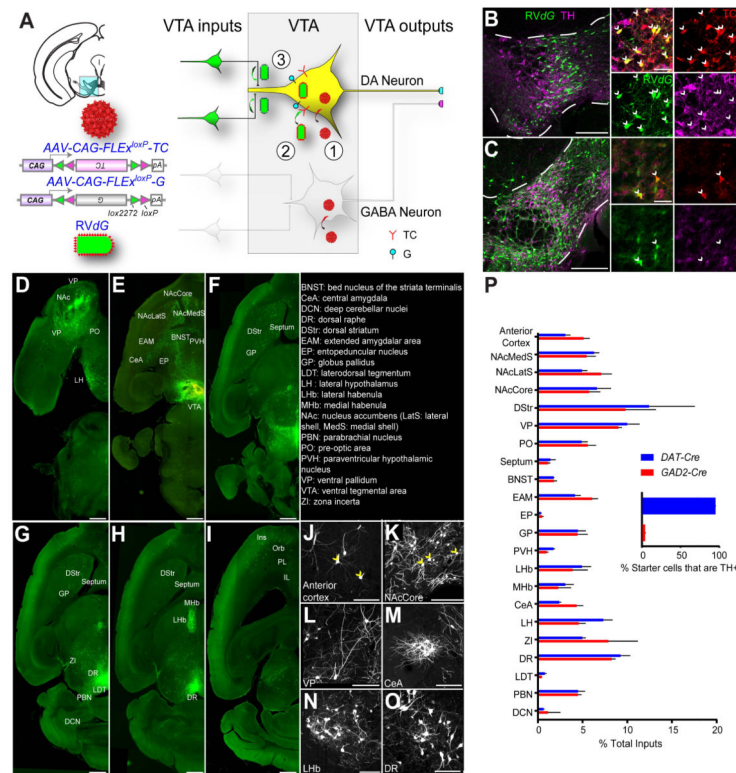
**Figure 1. Rabies-mediated Transsynaptic Tracing Reveals Inputs to VTA Dopamine (DA) and GABA Neurons**

(A) Schematic of rabies tracing, shown for *DAT-Cre*. Left, diagrams of the injection site (blue box highlights VTA) and the viruses used. (1) Injections of AAVs expressing Cre-dependent TVA-mCherry (TC) and rabies glycoprotein (G) were targeted unilaterally to the VTA. (2) Two weeks later, EnvA-pseudotyped, G-deleted, GFP-expressing rabies virus (RV*dG*) was injected into the same VTA site. (3) Five days were allowed for rabies to transduce and label synaptically-connected input neurons.

(B–C) In the VTA (between the dotted lines), most TC-expressing cells initiated in *DAT-Cre* mice co-stained with the anti-tyrosine hydroxylase (TH) antibody (B), while TC-labeled cells in *GAD2-Cre* animals did not (C). In the insets, arrows indicate TC-expressing cells. Green, GFP from RV*dG*; red, TC; magenta, TH immunoreactivity. Scale, 200 µm (100 µm for inset).

(D–I) Horizontal section series showing brain-wide distribution of input to VTA-DA neurons. Scale, 1 mm.

(J–O) High-magnification images of rabies-infected input neurons, including principal neurons in the cortex and striatal projection neurons in the NAcCore (yellow arrowheads). Scale, 100 µm.

(P) Quantification of inputs to VTA-DA or VTA-GABA neurons from *DAT-Cre* or *GAD2-Cre* mice, respectively. Data are shown as percent of inputs from a given region relative to total counted inputs throughout a given brain. While overall inputs to DA and GABA neurons are significantly different (p<0.01, Fisher's combined probability test), no individual input showed a significant preference for DA or GABA neurons (p>0.05 for all inputs, t-test with Holm-Sidak correction for multiple comparisons). Inset, 95% of starter

cells in the VTA of *DAT-Cre* mice are TH$^+$, while 4% in *GAD2-Cre* animals are TH$^+$; n=4 for each condition.

In this and all subsequent figures, error bars represent s.e.m.

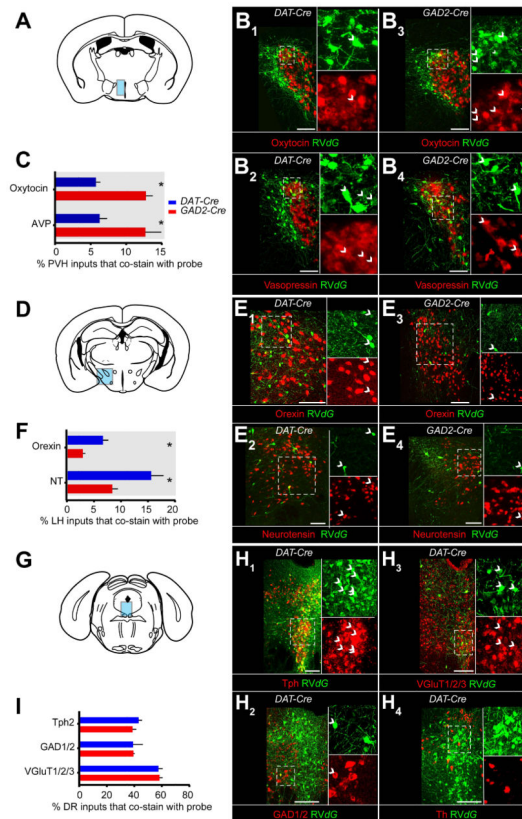See also Figure S1, S2, S4, S5, and Table S1–S3 for related data.

**Figure 2. VTA-DA and VTA-GABA Neurons Receive Synaptic Inputs from Diverse Cell Types**

(A) Coronal schematic showing the paraventricular hypothalamus (PVH, blue) where inputs to VTA-DA and -GABA neurons were examined for expression of the mRNAs encoding either oxytocin ($B_1$, $B_3$) or arginine vasopressin (AVP; $B_2$, $B_4$) precursors.

(B) Overlap of in situ hybridization (ISH) signals (red) with GFP from RV*dG* (green) was observed for inputs to both VTA-DA ($B_1$-$B_2$) and VTA-GABA ($B_3$-$B_4$) neurons. Arrowheads indicate cells co-labeled with ISH probe and GFP.

(C) Quantification of percentage of total rabies-labeled inputs in the PVH that co-stained with ISH probe. Both oxytocin+ (p<0.001, t-test) and AVP+ (p=0.02) neurons showed a preference for sending input to VTA-GABA neurons. n=6 (mice) for both probes in *DAT-Cre*, and n=5 for both probes in *GAD2-Cre*.

(D–F) ISH in the lateral hypothalamus (LH) for genes encoding orexin (hypocretin) or neurotensin (NT), analogous to panels A–C. (F) Both orexin neurons (p=0.0143) and NT neurons (p=0.03) showed a preference for VTA-DA neurons. n=4 for all.

(G–I) ISH in the dorsal raphe (DR) for genes encoding Tph2, GAD1/2, VGluT1/2/3, and TH, in *DAT-Cre* mice. No TH[+]/GFP^{+} neurons were observed. (I) Serotonin (p=0.27), GABA (p=0.97), and glutamate (p=0.84) neurons did not show a preference for VTA-DA or VTA-GABA neurons. n=4 for all. The combined fraction exceeded 100% because a large fraction of neurons were both vGluT3[+] and Tph2^{+}.

All statistics were t-tests. p-values were obtained with Holm-Sidak correction for multiple comparisons where applicable. Scale, 100 μm.
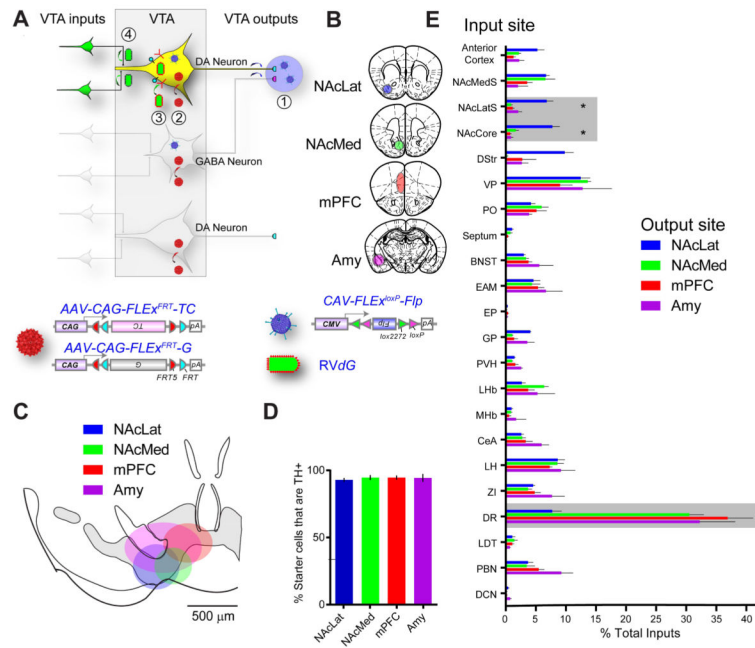
**Figure 3. cTRIO Analysis of the Input–Output Relationships of VTA-DA Neurons**

(A–B) Schematic of cTRIO experiments. (1) *CAV-FLEx$^{loxP}$-Flp* was injected into one of four output sites (coronal schematics in B). (2) On the same day, AAVs that express Flp-dependent TC and G were injected into the VTA. (3) Two weeks later, RV*d*G was injected into the VTA. (4) Five days later, histological analyses were performed.

(C) Average starter cell distributions at the VTA for four cTRIO conditions. The center of each oval represents the center of mass for starter cells, and the horizontal and vertical radii of the oval represent one standard deviation of starter cells in the medial–lateral and dorsal–ventral axes, respectively. See Figure S4 for more details.

(D) Percentage of starter cells that co-label with TH for each cTRIO condition.

(E) Whole-brain input data to each of the VTA neuronal populations defined by cTRIO (n=4 for each condition). Percentage of total inputs is plotted on the x-axis, and brain region on the y-axis. Brain regions with significant differences (p<0.05, 1-way ANOVA for each brain region, with Holm-Sidak correction for 22 1-way ANOVAs) are highlighted in gray. *: NAcLatS, NAcCore, and DR send significantly different fractional input to NAcLat compared to NAcMed, mPFC, and Amy (p<0.05, post-hoc pairwise comparisons with Holm-Sidak corrections for 6 comparisons). Because NAcLat-projecting VTA-DA neurons produce the most inputs (Table S1), the input distribution from NAcLat-based cTRIO resembles Figure 1P the most.

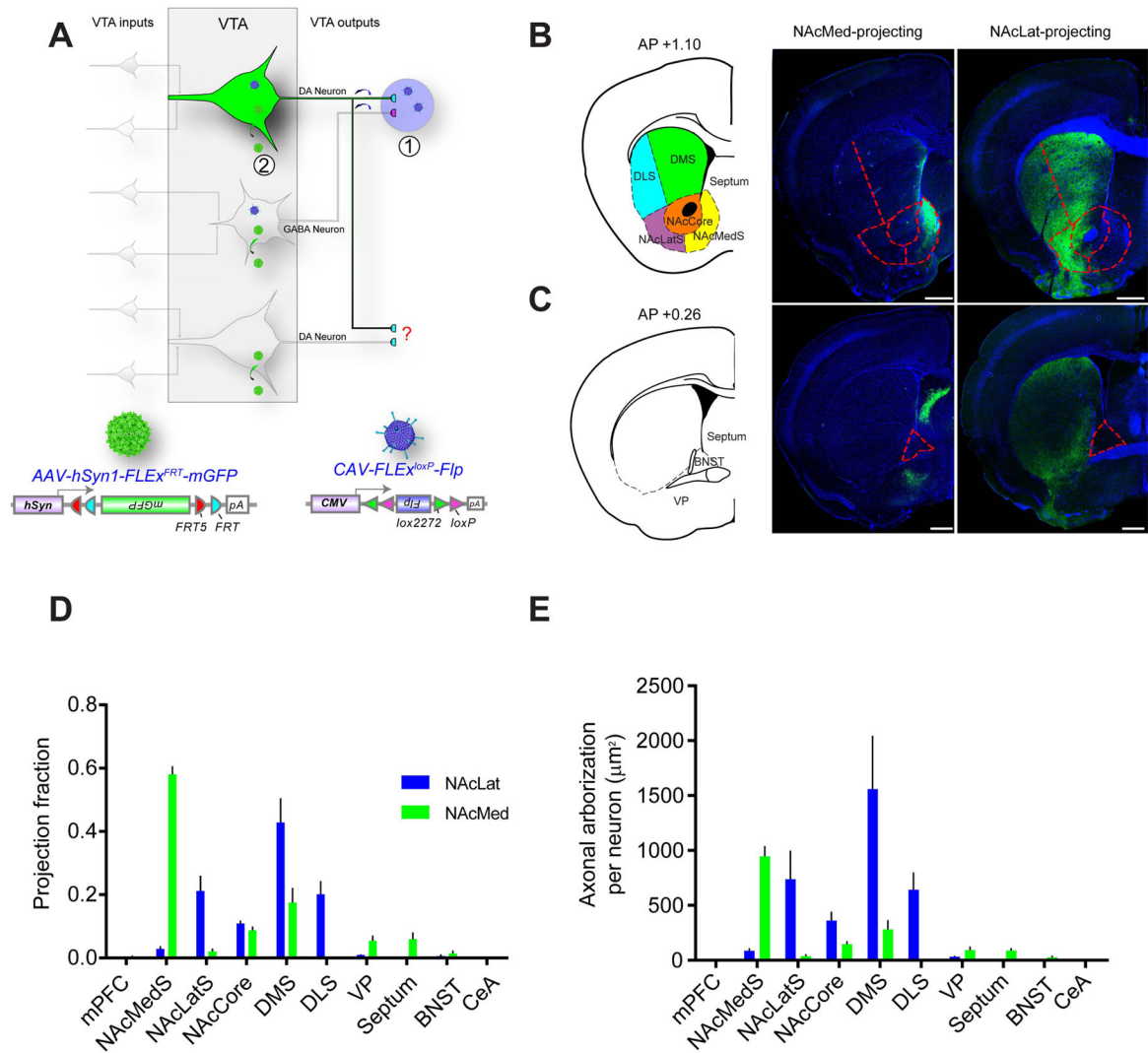See Figure 1 for abbreviation of anatomical regions, Figure S2–S4 and Table S1–S3 for related data.

**Figure 4. Axonal Arborization Analysis of NAcLat- and NAcMed-projecting VTA-DA Neurons**

(A) Schematic of experimental setup. (1) *CAV-FLEx$^{loxP}$-Flp* was injected into either the NAcLat or NAcMed. (2) On the same day, an AAV expressing Flp-dependent membrane-GFP was injected into the VTA. Brains were harvested two months later.

(B) Representative coronal sections showing axonal projections of NAcMed-projecting (middle) and NAcLat-projecting (right) VTA-DA neurons in the striatum, along with the atlas schematic (left). Dotted lines outline subdivisions of the striatum. DLS, dorsolateral striatum; DMS, dorsomedial striatum.

(C) Same as in (B) except more posterior coronal sections are shown. Dotted lines outline the BNST.

(D) Proportion of total arborization of NAcMed- and NAcLat-projecting VTA-DA neurons across 10 brain regions. An average of 349±80 VTA-DA neurons were labeled by targeting NAcMed (n=5), and 366±106 neurons by NAcLat (n=4).

(E) NAcLat-projecting DA neurons showed a broader arborization than NAcMed-projecting DA neurons, as evidenced by a greater area covered by labeled axonal arbors. Scale, 500 μm.
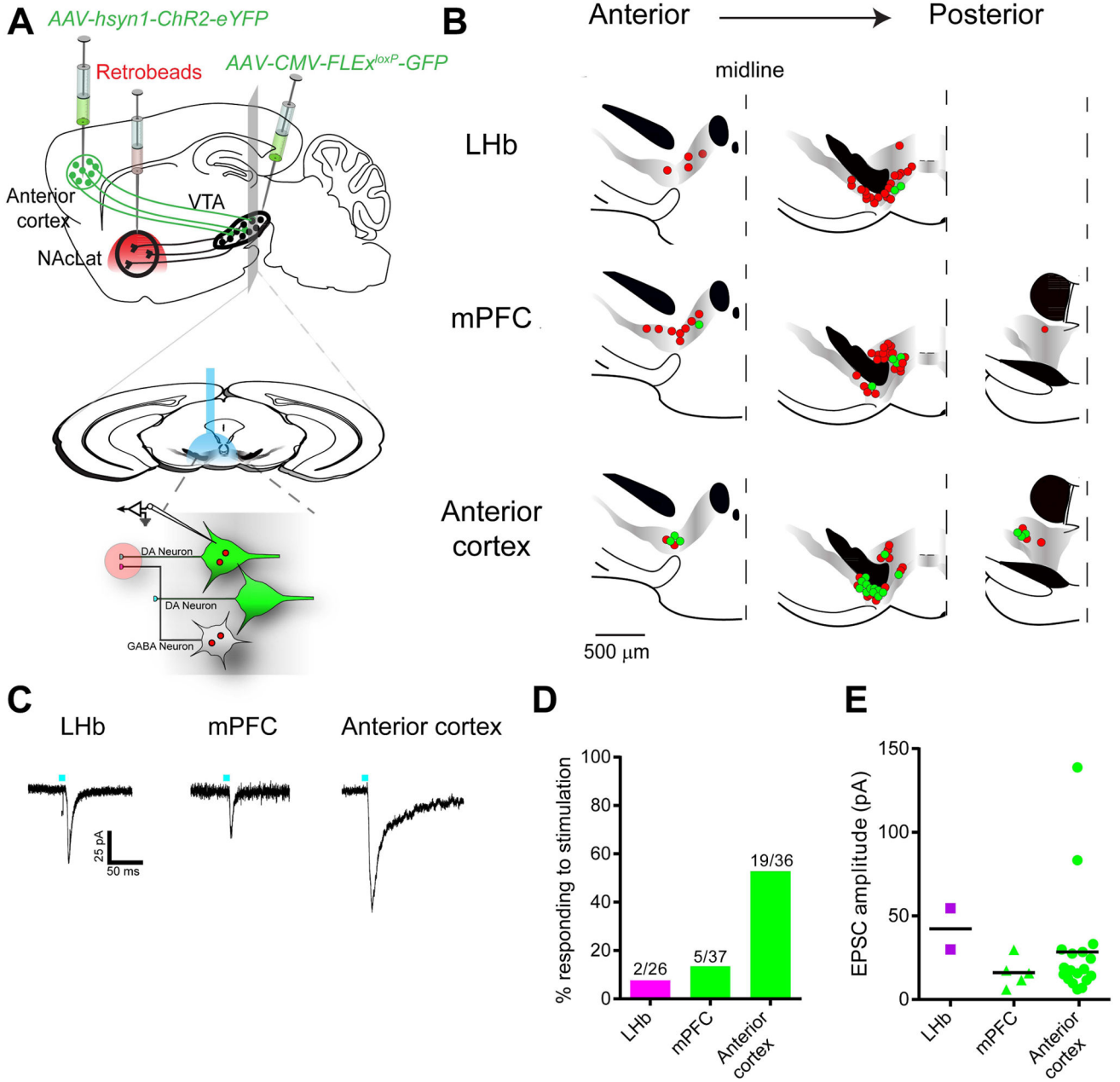
**Figure 5. Electrophysiological Validation of New Pathways Identified using cTRIO**

(A) Schematic of experimental setup. An AAV expressing ChR2-eYFP was injected into the lateral habenula (LHb), medial prefrontal cortex (mPFC), or anterior cortex (depicted), red retrobeads were injected into NAcLat, and *AAV-CMV-FLEx^loxP-GFP* into the VTA of a *DAT-Cre* mouse. Two months later, whole-cell recordings were conducted from GFP^+ retrobeads^+ neurons in acute VTA slices while photostimulating ChR2-expressing axons and terminals.

(B) Map of responding (green) and non-responding (red) cells to photostimulation.

(C) Sample excitatory postsynaptic currents (EPSCs) from identified VTA-DA neurons receiving inputs from the LHb, mPFC, or anterior cortex.

(D) Quantification of connectivity from each input site.

(E) Average EPSC amplitudes from responding cells at –60 mV in each experiment.

Colored shapes and black bars indicate individual values and the means, respectively.
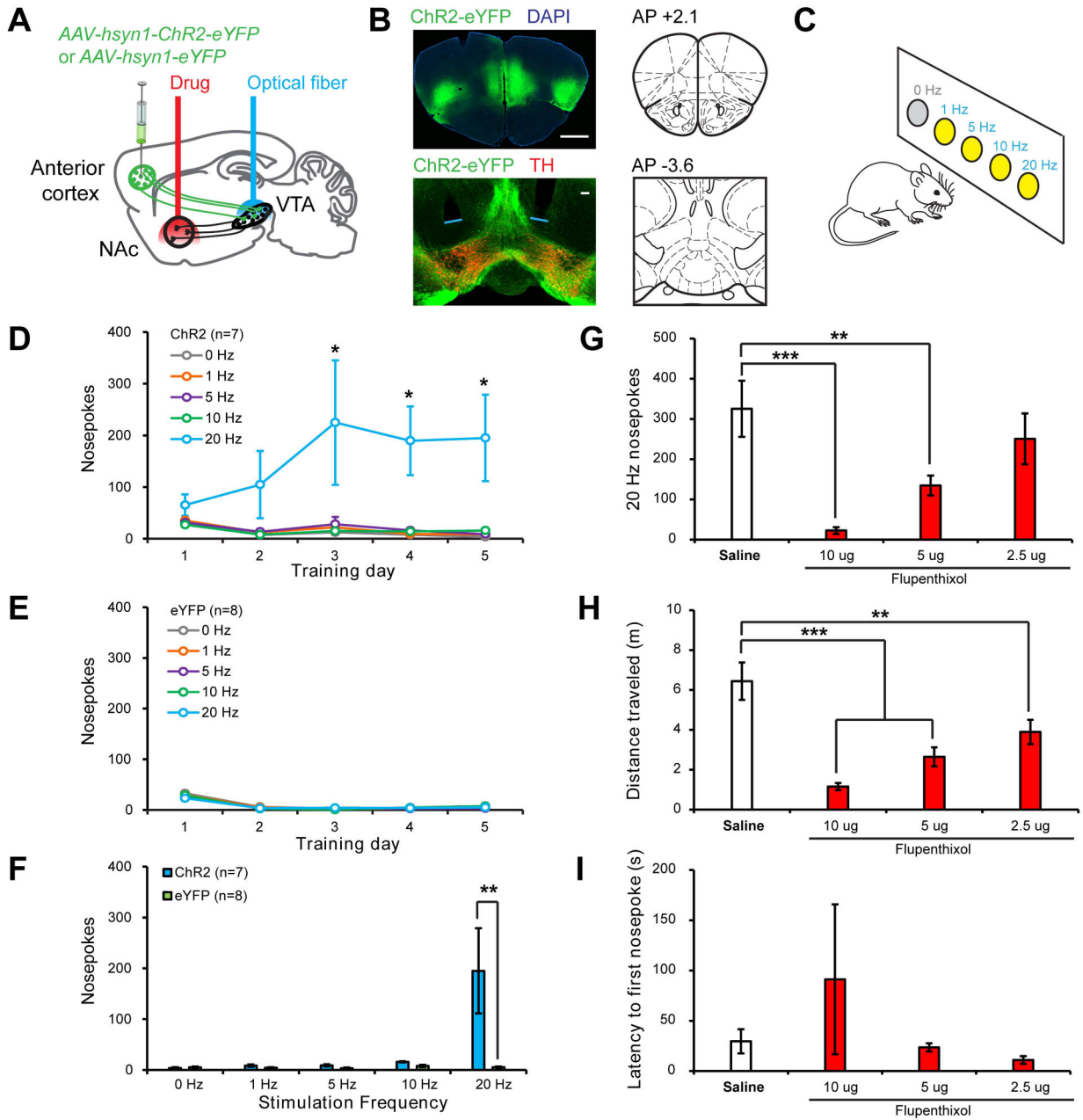
See Figure S5 for related data.

**Figure 6. Behavioral Function of the Anterior Cortex→VTA-DA→NAcLat Circuit**

(A) Schematic of experimental setup. An AAV expressing either ChR2-eYFP or eYFP was injected into the anterior cortex (medial and lateral sites) and optical fibers were implanted above the VTA so that anterior cortex axon terminals innervating the VTA could be optically stimulated. A guide cannula was also implanted targeting the NAcLat in all mice for drug delivery in some experiments. All manipulations were bilateral.

(B) Top, ChR2-eYFP expression following virus injection into anterior cortex. Scale, 1 mm. Bottom, ChR2-eYFP-expressing axon terminals in the VTA of the same mouse. Blue lines indicate optical fiber tips. Scale, 100 μm.

(C) Schematic of ICSS task. Mice were allowed to respond freely at 5 nosepoke ports for 1 hr per day over 5 training days. A response at 4 ports resulted in the delivery of a 2s train of light pulses at varying frequencies (1, 5, 10, 20 Hz); an LED in the back of the port was concurrently illuminated to serve as a visual cue indicating ongoing stimulation. Responses at a 5th control port (0 Hz) had no consequence. For the first training session, all nosepokes were baited to facilitate initial investigation.

(D) Mice expressing ChR2-eYFP (n=7) developed a strong preference for the 20 Hz port as compared to the 0 Hz control port (1-way Friedman repeated-measures ANOVA on ranks, main effect of nosepoke type p<0.006 on days 3–5; 20 Hz vs 0 Hz p<0.05, Tukey post-hoc tests).

(E) Mice expressing eYFP (n=8) responded at similarly low levels at all nosepoke ports (p>0.351, days 1–5).

(F) On training day 5, ChR2-eYFP mice made significantly more nosepokes at the 20 Hz port than eYFP mice (Mann-Whitney Rank-Sum test with Bonferroni correction, p=0.005), indicating that optical activation of the anterior cortex-VTA projection is reinforcing.

(G–I) Infusion of the non-selective dopamine receptor antagonist flupenthixol into the NAcLat dose-dependently decreased responding for 20 Hz stimulation of anterior cortex→VTA projections in ChR2-eYFP-expressing mice (n=5) (G; 1-way repeated-measures ANOVA, main effect of drug p<0.001; 10 Ag and 5 Ag flupenthixol vs. saline vehicle p<0.001 and p=0.01 respectively, Holm-Sidak post-hoc tests). Doses indicate amount of drug delivered per hemisphere in 0.25 μl saline. While locomotion was also concurrently decreased by flupenthixol (H; 1-way repeated-measures ANOVA, main effect of drug p<0.001; 10 μg, 5 μg and 2.5 μg flupenthixol vs. saline vehicle, p<0.001, p<0.001 and p=0.003 respectively, Holm-Sidak post-hoc tests) (H), the latency to make the first response was unaffected (I; p=0.482), indicating that mice were physically capable of performing nosepoke responses during behavioral sessions where flupenthixol was administered.

See Figure S6 for related data.